



Optics Letters

Ultra-wideband discrete Raman amplifier optimization for single-span S-C-L-band coherent transmission systems

PRATIM HAZARIKA,  MINGMING TAN,*  ALEKSANDR DONODIN,  MOHAMMAD PATEL, IAN PHILLIPS,  PAUL HARPER, AND WLADEK FORYSIAK 

Aston Institute of Photonic Technologies, Aston University, Birmingham B4 7ET, UK

*Corresponding author: m.tan1@aston.ac.uk

Received 12 September 2022; revised 8 November 2022; accepted 8 November 2022; posted 9 November 2022; published 13 December 2022

We experimentally compare the performance of two key ultra-wideband discrete Raman amplifier structures, a cascaded dual-stage structure and an in-parallel dual-band structure, in fully loaded S-C-L band coherent transmission systems over 70 km of single-mode fiber. Our results show that dual-band discrete Raman amplifier with minimized backreflections can effectively avoid unstable random distributed feedback lasing, reduce the noise figure, and therefore improve the transmission performance for signals at shorter wavelengths, versus the cascaded dual-stage structure. The average noise figure for S-band signals is 6.8 dB and 7.2 dB for the dual-band structure and cascaded dual-stage structure, respectively, while the average S-band Q^2 factor is similarly improved by 0.6 dB. Moreover, the cascaded dual-stage discrete Raman amplifier requires guard bands around the 1485-nm and 1508-nm pumps as the signal and pump wavelengths overlap, which results in a bandwidth loss of ~ 10 nm and reduces the potential net data throughput to 28.6 Tb/s for 30-GBaud DP-16QAM signals. However, the dual-band structure can utilize the bandwidth more effectively, which leads to a higher estimated net data throughput of 31.2 Tb/s.

Published by Optica Publishing Group under the terms of the [Creative Commons Attribution 4.0 License](https://creativecommons.org/licenses/by/4.0/). Further distribution of this work must maintain attribution to the author(s) and the published article's title, journal citation, and DOI.

<https://doi.org/10.1364/OL.475246>

Introduction. Recently, ultra-wideband optical amplification techniques have attracted significant interest to tackle the ever-increasing data demand in optical fiber communications, as alternatives to techniques to improve the spectral efficiency such as advanced modulation formats and space division multiplexing (SDM) using multi-core/mode fiber [1–4]. Discrete Raman amplifiers (DRAs) have been proposed and demonstrated to be a promising candidate to enable amplification for ultra-wideband transmission systems [5–7]. A crucial issue to address in using DRAs over a large bandwidth is the noise figure tilt resulting in signal performance degradation at shorter wavelengths due to increased thermally generated ASE noise when pumps are

spectrally close to the signal [6]. Iqbal *et al.* proposed a cascaded dual-stage discrete Raman amplifier structure which partitions the S-band and C + L-band pumps in the first and second amplifier stages, respectively [8]. This structure improves the noise figure and signal performance at shorter wavelengths, compared with a single stage S + C + L-band DRA, with all pumps on one fiber, resulting in stronger pump-to-pump interactions [9]. Another effective way of reducing such interaction is to separate the signals and pumps to different bands and allow them to be amplified in their corresponding bands simultaneously. However, it remains uninvestigated experimentally how the signal performs differently using an in-parallel dual-band structure or cascaded dual-stage amplifier, which becomes extremely crucial when optimizing the ultra-wideband transmission systems beyond the conventional C + L bands.

In this paper, for the first time to the best of our knowledge, we experimentally compare the performance of different DRA structures: cascaded dual-stage DRA and in-parallel dual-band DRA. For the in-parallel dual-band DRA, backreflections from the end connectors must be minimized to avoid the unstable random fiber lasing. Therefore, we include two setups for the dual-band DRA schemes, one with low-level, 4% backreflections from the FC/UPC end connector, and the other minimizing backreflections by adding an extra optical isolator. Our results show the dual-band DRA with backreflections suffers from unstable random fiber lasing due to distributed Rayleigh backscattering from the Raman gain fiber and 4% backreflection, once the Raman pump power exceeds a certain threshold. Beyond this threshold, unstable random lasing occurs which significantly limits the Raman gain in the S-band and degrades the signal transmission performance. In terms of the backreflection impact on DRA performance, the average Raman gain and noise figures in the S-band without backreflections were 15.3 dB and 6.8 dB, respectively, compared with only 12.5 dB and 8 dB with backreflections. For the cascaded dual-stage DRA, the average S-band gain and noise figure were 14.5 dB and 7.2 dB, respectively, 0.8 dB lower and 0.4 dB higher than for the best dual-band DRA performance (with an optical isolator mitigating the backreflections).

The transmission performance was studied using a 30-GBaud DP-16-QAM signal coupled with fully loaded channelized ASE

over S + C + L bands, for all the structures. The dual-band setup without backreflections performed the best with the average Q^2 factor of 14.2 dB in the S band, followed by cascaded dual-stage setup with the average Q^2 factor of 13.6 dB. The dual-band setup with backreflections showed the worst performance, giving a Q^2 factor of 11.8 dB. The Raman gain, noise figures, and transmission performances in C + L bands were very similar among the three schemes. Note, the cascaded dual-stage DRA required guard bands around the pumps at 1485 nm and 1508 nm, resulting in a loss of transmission window of ~10-nm bandwidth, which reduced the net data throughput to 28.6 Tb/s assuming the use of 30-GBaud DP-16QAM on all channels. As a comparison, no guard band was required from the dual-band DRA, improving the potential net data throughput to 31.2 Tb/s.

Experimental setup and characterization of DRA schemes. Figure 1 shows the experimental setup for the characterization of different DRA structures. To conduct the standalone characterization and the follow-on transmission experiment, we constructed a fully loaded channelized input spectrum extending from 1470 to 1605 nm covering the S-, C-, and L-bands, as illustrated in Fig. 1(a) [10].

The three different amplification schemes tested over 70 km of single-mode fiber (SMF) are illustrated in Fig. 1. Scheme 1 is a cascaded dual-stage DRA, which separated signal and pumps into two cascaded stages, S-band amplification followed by C + L band amplification [8], using 7.5 km of inverse dispersion fiber (IDF) in each stage. Three pump wavelengths (1365, 1385, 1405 nm) were used for the S-band stage, and five pump wavelengths (1425, 1445, 1465, 1485, 1508 nm) were used for the C + L band stage. Optical isolators and a circulator were used to prevent any backreflection from connectors and separated the two stages. The output spectrum of the cascaded dual stage is shown in Fig. 1(b). Figure 2(a) shows the net gain and

noise figure using the cascaded dual-stage DRA (Scheme 1) over 70 km of SMF. The average net gain for the whole S + C + L band was 13.9 dB, where the average net gain for the S-band was 14.5 dB. The averaged noise figure for the whole band was 6.5 dB, whereas the average noise figure for the S-band was 0.7 dB higher.

Schemes 2a and 2b are essentially the same scheme, that is, a dual-band DRA. Two paths were used to separate the S-band and C + L band, which led to no signal power transfer from the S-band to L-band in the amplifier section. In this case, four pump wavelengths were used in the S-band, including 1365 nm, 1385 nm, 1405 nm, and 1425 nm. Note, one additional pump at 1425 nm was used for the amplification of longer S-band signals (1510–1520 nm) in the dual-band configurations, while in the dual-stage configuration, this pump was available in the DRA’s second stage. For the C + L band, the pump wavelengths were the same as the dual-stage structure (1425, 1445, 1465, 1485, 1508 nm). A key difference between the two schemes is whether the backreflection from the output connector of the filter WDM (FWDM) in the S-band path was minimized. As shown in Scheme 2a, with no isolator between the IDF output WDM and the filter WDM, a half-open random fiber laser cavity was formed [11–13]. One side of the cavity was “open” due to the distributed Rayleigh backscattering of the 7.5-km IDF, and the other side was “closed” and fixed, due to the 4% Frenzel reflection of the FC/UPC connector at the output of FWDM. Figure 1(I) shows evidence of the unstable lasing, but the pump power was insufficient to exceed the threshold to achieve stable random lasing. Stable random fiber laser can be used for higher-order Raman amplification [11], but for discrete Raman, this random fiber lasing (even if it is stable) was not required as this is only a first-order Raman amplification. To avoid this unwanted lasing, the Raman pump powers were reduced, as

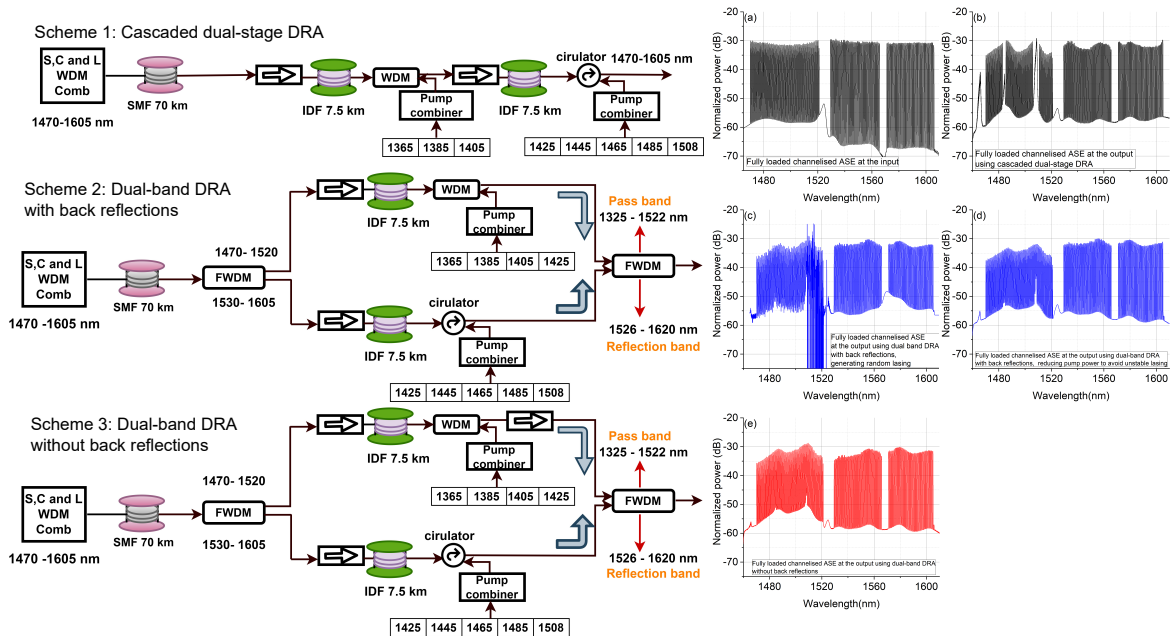


Fig. 1. Scheme 1, cascaded dual-stage DRA; Scheme 2a, dual-band DRA with backreflections; Scheme 2b, dual-band DRA without backreflections. (a) Fully loaded signal spectrum captured at the input of all three DRAs. (b) Spectrum received at the output of the cascaded dual-stage DRA. (c) Spectrum received at the output of the dual-band DRA with backreflections, due to the unstable random lasing formed by distributed Rayleigh backscattering from the IDF and the connector at the FWDM output; (d) Spectrum received at the output of the dual-band DRA, reducing the pump power to avoid unstable lasing. (e) Spectrum received at the output of the dual-band DRA without backreflections by inserting an isolator.

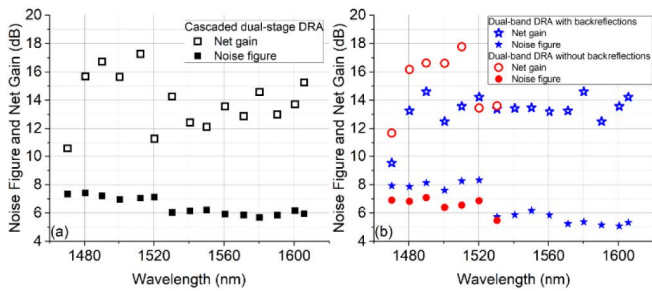


Fig. 2. Net Raman gain and noise figures in (a) Scheme 1, cascaded dual-stage DRA; (b) dual-band DRA with backreflections (Scheme 2a, blue) and without backreflections (scheme 2b, red).

Table 1. Pump Power and Wavelengths Used in Different DRAs

λ /nm	Power for Scheme 1	Power for Scheme 2a	Power for Scheme 2b
1365	432	275	366
1385	297	215	309
1405	103	165	224
1425 S band	N/A	234	326
1425 C band	289	450	450
1445	304	349	349
1465	269	216	216
1485	67	86	86
1508	112	72	72
Total	1,873	2,062	2,398

show in Table 1, and therefore the net Raman gain was reduced. The average gain for the whole band in Scheme 2a with backreflections was 13.3 dB, but the average gain for the S-band was 12.5 dB, more than 2 dB lower than using the cascaded dual-stage DRA. The overall noise figure was 6.5 dB, but the noise figure for the S-band was 8 dB, ~ 0.8 dB higher than using the cascaded dual-stage DRA. This is because the signal in the S-band suffered more thermal noise introduced from the pumps in the second stage as well as signal-to-signal power transfer to longer wavelengths. For the C+L band, there was no impact on the Raman gain or noise figure as the backreflections only occurred in the S-band path.

To fully minimize the backreflections and avoid the unstable random fiber lasing, an optical isolator was inserted between the WDM after the IDF and the FWDM in the S-band path, eliminating the half-open cavity, and leaving a fully-open cavity which requires much higher pump power to reach the random lasing threshold [13]. In this way, a higher Raman pump power was enabled and higher Raman gain was achieved. The output spectrum is shown in Fig. 1(e). The net Raman gain in the S-band for Scheme 2b without backreflections was 15.3 dB, ~ 0.8 dB higher than the dual-stage scheme and almost 3 dB higher than Scheme 2a. The average S-band noise figure was 6.8 dB, 0.4 dB lower than Scheme 1 (dual-stage) and 1.2 dB lower than Scheme 2a. The only disadvantage of the Scheme 2b DRA over Scheme 1 was the requirement of higher total Raman pump power, ~ 2.4 W versus 1.9 W.

Transmission results and discussions. To evaluate the transmission performance using the three different DRAs, we conducted a short-reach single-span experiment using coherent transmission over 70 km of SMF [14]. Figure 3 shows a

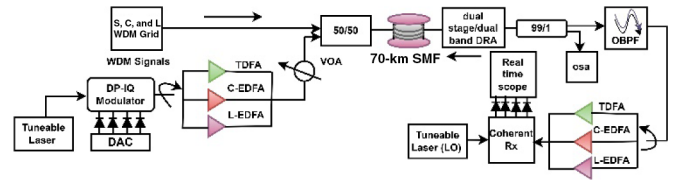


Fig. 3. Experimental setup for DP-16QAM coherent transmission systems using S + C + L band fully loaded channels with different DRAs over 70-km SMF.

detailed schematic diagram of the transmission setup. A narrowlinewidth tunable laser ranging from 1450 to 1650 nm was used as the channel-under-test (CUT) and fed into an LiNbO₃ modulator driven by 120-GSa/s digital-to-analog converter (DAC) to form a 30-GBaud DP-16QAM signal [15]. The modulated signal was then amplified by a suitable amplifier (S-band TDFA or C/L-band EDFA depending on the CUT). The WDM grid formed by channelized ASE from 1470 to 1605 nm was combined with the modulated signal via a 50/50 WDM coupler, which can potentially provide a total net data throughput of 31.6 Tb/s. The total signal power fed into the SMF was 16.2 dBm with approximately -5.2 dBm per channel. The average SMF loss was 14.8 dB which was compensated by the DRAs. The amplified signals were coupled using a 99/1 coupler to monitor the output spectrum and an optical filter was used to demultiplex the WDM signals. A receiver amplifier (S-band TDFA, C- or L-band EDFA) was used to provide constant power to the coherent receiver. The receiver was a standard dual-polarization coherent detection setup, and the signals were captured with four high-speed photodetectors using an 80-GSa/s, 36-GHz bandwidth real time oscilloscope for analog-to-digital conversion. Digital signal processing (DSP) was performed offline with standard algorithms for signal recovery and linear impairments compensation. Q^2 factors were calculated from error counting and averaged over two million bits.

Figure 4 shows the Q^2 factor performance in two cases: back-to-back (B2B) and using three DRAs over 70 km of SMF. In the B2B cases, no DRAs were used so the performance was very similar. However, the transmission performances were different with the DRA. The average Q^2 factor across the S + C + L band was 14.7 dB with a relatively small variation of 3.1 dB with an average Q^2 factor of 13.6 dB in the S-band. For the dual-band scheme with backreflections (Scheme 2a), the Raman gain in the S-band was limited due to the random lasing and therefore a worse transmission performance was observed. The average Q^2 factor over the whole band was 14.1 dB with a large variation of 5.4 dB, and an average Q^2 factor of only 11.8 dB for the S-band, 1.8 dB lower than cascaded dual-stage DRA (Scheme 1). Once the backreflection from the end connector was minimized to avoid the random lasing cavity, the transmission performance was improved because of the lower NF of the S-band signals in the dual-band structure, in comparison with the cascaded dual-stage where the S-band signals suffered from the strong thermal noise generated from the pumps in the second stage of the cascaded DRA and signal-to-signal power transfer to longer wavelength channels [6,16]. The average Q^2 factor using Scheme 2b in the S-band was 14.2 dB, 0.6 dB higher than the dual-stage DRA (Scheme 1), and 2.4 dB higher than the dual-band DRA with backreflections (Scheme 2a). Our experimental results show that, with proper measures to reduce backreflections

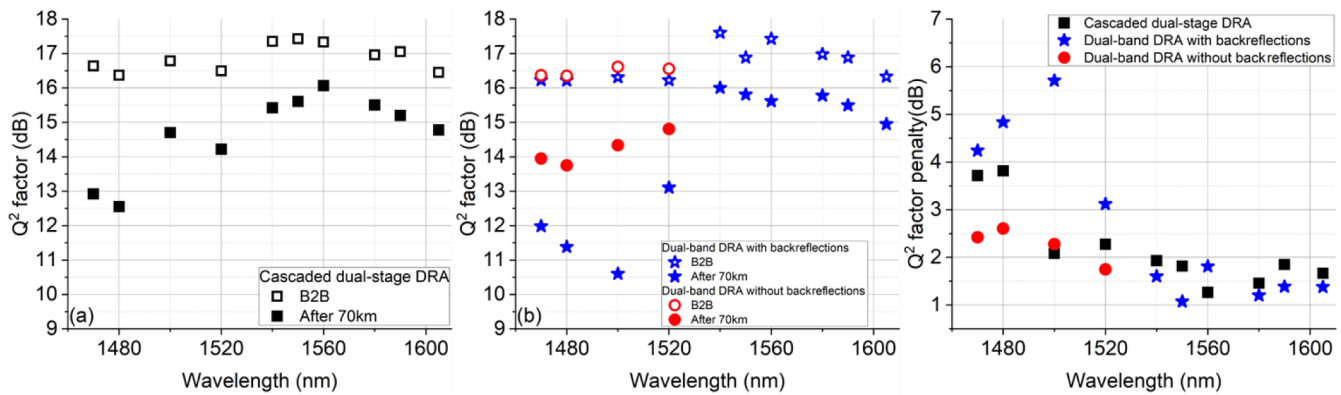


Fig. 4. (a) Q^2 factors of all the measured channels from 1470 nm to 1605 nm in back-to-back and using cascaded dual-stage (Scheme 1) DRA over 70-km SMF; (b) Q^2 factors of all the measured channels from 1470 nm to 1605 nm in back-to-back and using a dual-band DRA over 70-km SMF (Schemes 2a and 2b.); (c) Q^2 factor penalty between back-to-back and using three DRA schemes.

from the end connector, the dual-band DRA gave better transmission performance than the cascaded dual-stage DRA, which is particularly important to design an ultra-wideband transmission system enabled by DRAs. Moreover, based on the transmitted signal in this experiment, for dual-stage DRAs, as the signal and pump wavelengths overlapped at 1485 nm and 1508 nm, two guard bands (~ 5 nm each) around these were required which blocked parts of the transmission window. Using a dual-band DRA with proper mitigation of backreflections improved the potential net data throughput from 28.6 Tb/s to 31.2 Tb/s, assuming the use of 30-GBaud DP-16QAM signal channels. However, if the transmitted signal can be “seamless” over the S-C-L-band, there would be a guard band of 4 nm from FWDMs in the dual-band DRA, in comparison with ~ 10 nm in the cascaded dual-stage DRA.

Conclusion. We have demonstrated the experimental characterization of two important discrete Raman amplifier structures, a cascaded dual-stage DRA and an in-parallel dual-band DRA, using 30-GBaud DP-16-QAM over S+C+L bands (across 135-nm bandwidth) over 70-km SMF. Our results show that minimized backreflections are required to prevent unstable random fiber lasing which subsequently limits the net Raman gain. We also show that the dual-band DRA without backreflections can more effectively reduce the signal-to-signal power transfer to longer wavelengths and the noise figures at short wavelengths, in comparison with the cascaded dual-stage DRA. Our transmission results with the dual-band DRA with no backreflections gave an average Q^2 factor of 14.2 dB in the S-band, while the cascaded dual-stage DRA gave 13.6 dB. The average Q^2 factor across C- and L-bands gave similar Q^2 factors. Furthermore, for the cascaded dual-stage DRA, the signal and the pumps overlapped in the first stage of the DRA, and therefore guard bands around the pump wavelengths were required, restricting the total signal transmission window. As such, using the dual-band DRA without backreflections leads to an improvement in the potential net data throughput by 2.6 Tb/s, recovering the blocked transmission window of ~ 10 nm when using the dual-stage DRA.

Funding. H2020 Marie Skłodowska-Curie Actions (814276); Royal Society (IEC\NSFC\211244); Engineering and Physical Sciences Research Council (EP/V000969/1).

Acknowledgments. We thank Socionext for providing DACs, Lumentum for providing modulators, and Coherent for providing pump lasers.

Disclosures. The authors declare no conflicts of interest.

Data availability. Data underlying the results presented in this paper are available in Ref. [17].

REFERENCES

- B. J. Puttnam, R. S. Luis, G. Rademacher, Y. Awaji, and H. Furukawa, *J. Lightwave Technol.* **40**, 1633 (2022).
- L. Rapp and M. Eiselt, *J. Lightwave Technol.* **40**, 1579 (2022).
- A. Ghazisaeidi, I. Fernandez de Jauregui Ruiz, R. Rios-Müller, L. Schmalen, P. Tran, P. Brindel, A. C. Meseguer, Q. Hu, F. Buchali, G. Charlet, and J. Renaudier, *J. Lightwave Technol.* **35**, 1291 (2017).
- L. Galdino, A. Edwards, W. Yi, E. Sillekens, Y. Wakayama, T. Gerard, W. S. Pelouch, S. Barnes, T. Tsuritani, R. I. Killey, D. Lavery, and P. Bayvel, *IEEE Photonics Technol. Lett.* **32**, 1021 (2020).
- M. A. Iqbal, L. Krzczanowicz, I. Phillips, P. Harper, and W. Forsysiak, in *Optical Fiber Communication Conference (OFC) 2020, OSA Technical Digest* (Optica Publishing Group, 2020), paper W3E.4.
- S. Liang, S. Jain, L. Xu, K. R. H. Bottrill, N. Taengnoi, M. Guasoni, P. Zhang, M. Xiao, Q. Kang, Y. Jung, P. Petropoulos, and D. J. Richardson, *J. Lightwave Technol.* **39**, 1458 (2021).
- L. Krzczanowicz, M. A. Iqbal, I. Phillips, M. Tan, P. Skvortcov, P. Harper, and W. Forsysiak, *Opt. Express* **26**, 7091 (2018).
- M. A. Iqbal, L. Krzczanowicz, I. Phillips, P. Harper, and W. Forsysiak, in *Optical Fiber Communication Conference (OFC) 2020, OSA Technical Digest* (Optica Publishing Group, 2020), paper W4B.2.
- M. A. Iqbal, P. Harper, and W. Forsysiak, in *Advanced Photonics 2018, OSA Technical Digest (online)* (Optica Publishing Group, 2018), paper NpTh1H.2.
- P. Hazarika, M. Tan, A. Donodin, I. Phillips, P. Harper, M. Li, and W. Forsysiak, in *Optical Fiber Communication Conference (OFC)* (Optica Publishing Group, 2022), paper Tu3E.2.
- M. Tan, P. Rosa, S. T. Le Md., A. Iqbal, I. D. Phillips, and P. Harper, *Opt. Express* **24**, 2215 (2016).
- W. L. Zhang, Y. J. Rao, J. M. Zhu, Z. X. Yang, Z. N. Wang, and X. H. Jia, *Opt. Express* **20**, 14400 (2012).
- Z. Wang, H. Wu, M. Fan, L. Zhang, Y. Rao, W. Zhang, and X. Jia, *IEEE J. Sel. Top. Quantum Electron.* **21**, 10 (2015).
- M. Tan, M. A. Iqbal, T. T. Nguyen, P. Rosa, L. Krzczanowicz, I. D. Phillips, P. Harper, and W. Forsysiak, *Sensors* **21**, 6521 (2021).
- R. Emmerich, M. Sena, R. Elschner, C. Schmidt-Langhorst, I. Sackey, C. Schubert, and R. Freund, *J. Lightwave Technol.* **40**, 1360 (2022).
- G. Saavedra, M. Tan, D. J. Elson, L. Galdino, D. Semrau, M. A. Iqbal, I. D. Phillips, P. Harper, A. Ellis, B. C. Thomsen, D. Lavery, R. I. Killey, and P. Bayvel, *J. Lightwave Technol.* **35**, 4809 (2017).
- M. Tan, P. Hazarika, W. Forsysiak, P. Harper, A. Donodin, and I. Phillips, “Ultra-wideband discrete Raman amplifier optimisation for single-span S-C-L-band coherent transmission systems,” *Aston Research Explorer* (2022), <https://doi.org/10.17036/researchdata.aston.ac.uk.00000589>.